Mechanical properties of additively manufactured octagonal honeycombs

Hedayati, R.; Sadighi, M.; Mohammadi-Aghdam, M.; Zadpoor, A. A.

DOI
10.1016/j.msec.2016.08.020

Publication date
2016

Document Version
Accepted author manuscript

Published in
Materials Science and Engineering C: Materials for Biological Applications

Original article

Mechanical properties of additively manufactured octagonal honeycombs

R. Hedayati[1,2*], M. Sadighi[1], M. Mohammadi-Aghdam[1], A.A. Zadpoor[2]

[1]*Department of Mechanical Engineering, Amirkabir University of Technology (Tehran Polytechnic), Hafez Ave, Tehran, Iran*
[2]*Department of Biomechanical Engineering, Faculty of Mechanical, Maritime, and Materials Engineering, Delft University of Technology (TU Delft), Mekelweg 2, 2628 CD, Delft, The Netherlands*

[1] Corresponding author, email: rezahedayati@gmail.com, r.hedayati@tudelft.nl, rezahedayati@aut.ac.ir, Tel: +31-15-2781021.

Abstract

Honeycomb structures have found numerous applications as structural and biomedical materials due to their favourable properties such as low weight, high stiffness, and porosity. Application of additive manufacturing and 3D printing techniques allows for manufacturing of honeycombs with arbitrary shape and wall thickness, opening the way for optimizing the mechanical and physical properties for specific applications. In this study, the mechanical properties of honeycomb structures with a new geometry, called octagonal honeycomb, were investigated using analytical, numerical, and experimental approaches. An additive manufacturing technique, namely fused deposition modelling, was used to fabricate the honeycomb from polylactic acid (PLA). The honeycombs structures were then mechanically tested under compression and the mechanical properties of the structures were determined. In addition, the Euler-Bernoulli and Timoshenko beam theories were used for deriving analytical relationships for elastic modulus, yield stress, Poisson's ratio, and buckling stress of this new design of honeycomb structures. Finite element models were also created to analyse the mechanical behaviour of the honeycombs computationally. The analytical solutions obtained using Timoshenko beam theory were close to computational results in terms of elastic modulus, Poisson's ratio and yield stress, especially for relative densities smaller than 25%. The analytical solutions based on the Timoshenko analytical solution and the computational results were in good agreement with experimental observations. Finally, the elastic properties of the proposed honeycomb structure were compared to those of other honeycomb structures such as square, triangular, hexagonal, mixed, diamond, and Kagome. The octagonal honeycomb showed yield stress and elastic modulus values very close to those of regular hexagonal honeycombs and lower than the other considered honeycombs.

Keywords: Octagonal honeycomb; Timoshenko beam theory; Analytical relationships; Porous structures.

1. INTRODUCTION

Cellular solids have been widely studied as temporary or permanent scaffolds in tissue engineering [1, 2]. In general, cellular solids can be categorized into at least two main groups: foams and honeycombs. Foams have complex 3D micro-structural geometries with usually irregular unit cell shapes [3]. Honeycombs, on the other hand, possess in-plane tessellated and regular microstructures that form lightweight structures. The advent of additive manufacturing techniques made it possible to easily manufacture cellular solids with novel designs and precisely controlled micro-architectures. Several recent studies have investigated the mechanical and biological properties of additively manufactured 3D porous biomaterials with different unit cell types and densities [4-6]. To integrate well within the host tissue, tissue-substituting biomaterials should provide enough space for *de novo* tissue regeneration while exhibiting stiffness values close to the native tissue they replace. Having a micro-architecture similar to that of the native tissue, e.g. bone, could help tissue-substituting biomaterials to better mimic the mechanical response of the native tissue they replace. The microstructure of trabecular bone is shown to be close to that of honeycombs with thick walls in certain high density areas [7]. Recently, additive manufacturing techniques have been used for fabrications of biomedical implants based on honeycomb structures [8, 9]. Moreover, collagen scaffold with honeycomb-like micro-structure have been used for *in vitro* cell culture and *in vivo* studies [10-12].

In this study, we investigate the in-plane mechanical properties of a new design of honeycomb structures. Natural honeycombs constituting the cancellous bone, cork, or wood are usually loaded in in-plane [13]. Understanding the in-plane mechanical properties of honeycomb structures not only helps us better understand the form-function relationship in biological materials but could be also used for better design and (additive) manufacturing of tissue-substituting biomaterials.

Several experimental [14-21] and numerical [22-27] works have been published on the in-plane deformation of honeycombs. Hexagonal shape is the most widely studied geometry among the honeycombs. However, other types of honeycombs have also been investigated by other researchers [28]. Torquato et al. [29] investigated the effective linear elastic properties of honeycombs with square, hexagonal, and triangular cell shapes using two different approaches, namely homogenization theory and discrete network analyses, in order to establish rigorous bounds on the effective elastic modulus of honeycombs in terms of the thermal conductivity and vice versa [28]. The effective Young's modulus of triangular cell honeycombs was studied by Gulati [30] with reference to thermal shock resistance.

In addition to numerical and experimental studies, several analytical relationships have also been obtained for honeycombs with different micro-architectures. Analytical relationships provide fast (and accurate) estimation of the mechanical properties of honeycombs. Moreover, analytical models allow for better understanding of the various geometric aspects and physical mechanisms behind the mechanical behaviour of rationally designed materials such as honeycombs. For example, using analytical relationships, the user could quickly find the optimal micro-architecture of a honeycomb structure using simple optimization algorithms. The first analytical work published on the in-plane mechanical properties of honeycombs was performed by El-Sayed et al. [31] in which the elastic properties of unfilled and filled hexagonal honeycomb sheets under in-plane loading and out-of-plane bending were studied. However, their work had "numerous small errors" [13]. In 1982, Gibson et al. [13] obtained analytical relationships for different mechanical properties of *hexagonal* honeycombs (E_1, E_2, υ_{12}, υ_{21}, σ_{y1}, σ_{y2}, G, and σ_{el}). Their analytical results showed excellent agreement with their experimental results for both the rubber- and metal-made honeycombs but only for small values of relative density. A few other analytical studies [21, 32-34] were carried out to improve the Gibson et al.'s relationships for hexagonal honeycombs. Seven

other types of honeycomb cell shapes (square, triangular, hexagonal, Kagome, mixed, diamond, and rectangular) were investigated in a study by Wang and McDowell [28] using simple beam or column/truss elements, including linear and nonlinear theories to explore in-plane effective elastic stiffness and initial yield strength.

In this paper, a design for honeycomb-shaped pores referred to as octagonal, is introduced and its mechanical response is studied in the elastic range. An additive manufacturing technique, namely fused deposition modelling, was used to fabricate the honeycombs from polylactic acid (PLA). The honeycomb structures were then mechanically tested under compression and the mechanical properties of the structures were determined. The elastic modulus, Poisson's ratio, yield stress, and buckling stress of this structure is obtained analytically. The Euler-Bernoulli and Timoshenko beam theories are used for deriving the analytical relationships. Two finite element (FE) models are also created, one consisting of ¼ of a unit cell with periodic boundary conditions and the other consisting of a large set of unit cells. The experimental, analytical, and computational results are compared with each other.

2. MATERIALS AND METHODS

2.1. Experimental tests

We used an additive manufacturing technique, namely fused deposition modeling, to create octagonal honeycomb structures. Three samples from each relative density were manufactured and were mechanically tested under compression (Figure 5). The wall thickness to length ratios of the samples were varied between $t/l = 0.2727$, $t/l = 0.4091$, $t/l = 0.5454$, and $t/l = 0.6817$ to create four different relative densities. The specimens were made of poly-lactic acid (PLA) using 5th generation Replicator Desktop Makerbot 3D printers. All the samples had heights and widths of 77.26 mm and depths of 25 mm. The mechanical tests were done using Instron ElectroPuls E10000 machine with a 10kN load cell.

The samples were compressed with a displacement rate of 6 mm/min. The test procedures followed the specifications laid out by the ISO standard 13314:2011

To have a better impression of the elastic modulus and yield stress parameters, their normalized values (i.e., ratio of their value in the honeycomb structure to their corresponding value in the bulk material) are reported in the following. The mechanical properties of the bulk material are required when calculating the normalized values of elastic modulus and yield stress. Cylindrical specimens were created from the same PLA materials and were tested under compressive loading to determine their mechanical properties. The measured elastic modulus and yield stress of blue filaments were $E_s = 1.962 \pm 0.069\ GPa$ and $\sigma_{y_s} = 56.204 \pm 1.2127\ MPa$, respectively.

2.2. Relative density

Relative density is defined as the ratio of the density of a porous structure to the density of the material it is made of. Expressing the mechanical properties of a porous structure in terms of its relative density would be helpful in comparing its mechanical properties with those of other porous structures with different morphologies. In order to obtain the relative density, the volume of the bulk material present in one unit cell must be divided by the total volume occupied by the unit cell. Since the depth of the walls are constant throughout honeycomb structures, finding the filled and total areas of a unit cell in the cross-section of the lattice structure is sufficient (see2 Figure 1). If the cell walls are assumed to be thin enough, the area occupied by the materials constructing the walls of a unit cell is $(4lt + 4lt/2) = 6lt$. The total area of a unit cell is $l^2\left(\sqrt{2}+1\right)^2$. Consequently, the approximate relative density of an octagonal honeycomb is obtained as

$$\mu = \frac{6}{\left(\sqrt{2}+1\right)^2}\left(\frac{t}{l}\right) \tag{1}$$

The exact area occupied by the material constructing the walls of a unit cell is (Figure 1)

$$A_m = 8\left\{\frac{1}{2}\left(\frac{l}{2}-\frac{t\sqrt{2}}{2}+\frac{l}{2}-\frac{t\sqrt{2}}{2}+\frac{t}{2}\right)\frac{t}{2}+\frac{1}{2}\left(\frac{l}{2}+\frac{t}{2}+\frac{l}{2}-\frac{t}{2}\right)t\right\} \quad (2)$$

or

$$A_m = 2\left\{\left(l-t\sqrt{2}+\frac{t}{2}\right)t+2lt\right\} = 2t\left\{3l+\frac{t}{2}-t\sqrt{2}\right\} \quad (3)$$

and the area of a unit cell is again $l^2\left(\sqrt{2}+1\right)^2$. Therefore, the exact relative density of this structure is calculated as

$$\mu = \frac{2t\left\{3l+\frac{t}{2}-t\sqrt{2}\right\}}{l^2\left(\sqrt{2}+1\right)^2} = \frac{\frac{2t}{l}\left(3+\frac{t}{2l}-\frac{t}{l}\sqrt{2}\right)}{\left(\sqrt{2}+1\right)^2} \quad (4)$$

2.3. Euler-Bernoulli beam theory

In this section, we use the Euler-Bernoulli beam theory to derive analytical relationships for the elastic modulus, Poisson's ratio, and yield stress of an octagonal honeycomb structure as functions of the elastic modulus and yield stress of the matrix material (E_s, σ_{y_s}) and the relative density (μ) of the honeycomb.

Each of the unit cells constructing a 2D lattice structure (Figure 2) consists of two vertical, two horizontal, and four inclined edges. Due to the symmetry existent in the octagonal structure (Figure 2), considering ¼ of the structure (here the lower right portion) is sufficient for the analytical study (Figure 3a). If the total load applied to each unit cell is F, then the axial load applied to each vertical edge is $F/2$. The load applied to edge CD is $F/2$, and since the lattice structure is free to move laterally, the horizontal loads are zero. Due to the symmetry existent between each of two adjacent cells, the vertical and horizontal edges have to remain vertical and horizontal during elastic deformation. That is, if one of the noted edges rotates by $\theta°$, satisfying the symmetry conditions requires that it rotates $-\theta°$ in the adjacent cell. The rotation $-\theta°$ equals $\theta°$, only if $\theta = 0$. That holds only for the vertical and horizontal edges, because they are the only edges that are shared between adjacent cells. A concentrated

moment must have been applied to vertex C of edge CD by the adjacent cell located in the right side of the cell (Figure 3a) to keep the angle of vertex C unchanged. A moment with equal magnitude and reverse directions is applied by the cell to the noted edge of the right cell due to symmetry.

To calculate the displacements and rotations of the inclined edge (edge BC in Figure 3a), its free body diagram is plotted (Figure 3b). Edge AB must remain horizontal and, thus, the angle of vertex B must remain unchanged. Edge BC can therefore be considered as a cantilever beam at the end of which an axial load $F/2\sin\theta$, a lateral load $F/2\cos\theta$, and a moment M are applied, where $\theta = \pi/4$. As already stated, the loads $F/2\sin\theta$ and $F/2\cos\theta$ are imposed on edge BC by edge CD of the cell, while moment M is applied by the adjacent cell located in the right side of the cell. Since the vertical edge remains vertical, and given that angle C must remain constant, the rotation of beam BC at its end C must be zero after deformation. The axial load $F/2\sin\theta$ does not rotate the end C. Therefore, the rotations produced by the lateral load $F/2\cos\theta$ and the moment M must be equal and in the reverse directions from which the value of M can be calculated as:

$$\frac{\frac{F}{2}\frac{\sqrt{2}}{2}l^2}{2E_sI} = \frac{Ml}{E_sI} \qquad \Rightarrow \qquad M = \frac{Fl\sqrt{2}}{8} \tag{5}$$

where $I = \frac{1}{12}bt^3$ is the area moment of inertia of the edges in which b is the depth of the honeycomb structure in the out-of-plane direction. In order to obtain the vertical strain of the unit cell as a function of the applied load F (which is necessary for obtaining the elastic modulus and Poisson's ratio of the unit cell), first the vertical component of the structure displacement must be obtained. Decrease in the length of half of the vertical edge CD (i.e., CC`) is

$$\delta_{CC`} = \frac{\frac{F}{2}\frac{l}{2}}{\frac{A}{2}E_s} = \frac{Fl}{2AE_s} \tag{6}$$

where $A = bt$ is the cross-sectional area of the edges. The lateral load $F/2\cos\theta$ tends to decrease the length GC (Figure 3b) by

$$\delta_{BC_{F,bending}} = \frac{\frac{F}{2}\frac{\sqrt{2}}{2}l^3}{3E_sI}\frac{\sqrt{2}}{2} = \frac{Fl^3}{12E_sI} \tag{7}$$

On the other hand, the moment M tends to increase the length GC (Figure 3b) by

$$\delta_{BC_M} = \frac{Ml^2}{2E_sI}\frac{\sqrt{2}}{2} \tag{8}$$

Substituting M from Eq. (5) into Eq. (8) gives

$$\delta_{BC_M} = \frac{Fl^3}{16E_sI} \tag{9}$$

Finally, the axial load $F/2\,sin\,\theta$ tends to decrease the length GC (Figure 3b) by

$$\delta_{BC_{F,axial}} = \frac{\frac{F}{2}\frac{\sqrt{2}}{2}l}{AE_s}\frac{\sqrt{2}}{2} = \frac{Fl}{4AE_s} \tag{10}$$

Therefore, the total vertical displacement of the unit cell is

$$\delta_{uc} = 2\left(\delta_{CC`} + \delta_{BC_{F,axial}} + \delta_{BC_{F,bending}} - \delta_{BC_M}\right) = 2\left(\frac{Fl}{2AE_s} + \frac{Fl}{4AE_s} + \frac{Fl^3}{12E_sI} - \frac{Fl^3}{16E_sI}\right) \tag{11}$$

which after being simplified becomes

$$\delta_{uc} = \frac{3Fl}{2AE_s} + \frac{Fl^3}{24E_sI} \tag{12}$$

In order to find the elastic modulus of the octagonal honeycomb structure, the simple equation $E = \frac{F\,L_{uc}}{A_{uc}\delta_{uc}}$ can be used in which F is the load applied to the unit cell, and $L_{uc} = \left(1+\sqrt{2}\right)l$ and $A_{uc} = bl\left(1+\sqrt{2}\right)$ are the length and the cross-section area of the unit cell, respectively. Substituting Eq. (12) in $E = \frac{F\,L_{uc}}{A_{uc}\delta_{uc}}$ gives the elastic modulus of the octagonal honeycomb structure

$$E = \frac{F}{b\left[\frac{3Fl}{2AE_s} + \frac{Fl^3}{24E_sI}\right]} \tag{13}$$

and the relative elastic modulus is

$$E_\mu = \frac{E}{E_s} = \frac{1}{b\left[\frac{3l}{2A} + \frac{l^3}{24I}\right]} = \frac{2t}{l\left[3 + \left(\frac{l}{t}\right)^2\right]} \tag{14}$$

For obtaining the Poisson's ratio, it is first necessary to calculate the lateral displacement of the unit cell. The lateral displacement of the unit cell is twice the horizontal displacement of point C in Figure 3, which is given by

$$\delta_{lateral} = 2\left(-\delta_{BC_F,axial} + \delta_{BC_F,bending} - \delta_{BC_M}\right) \tag{15}$$

Substituting Eqs. (7), (9) and (10) into Eq. (15) gives

$$\delta_{lateral} = 2\left(-\frac{Fl}{4AE_s} + \frac{Fl^3}{12E_sI} - \frac{Fl^3}{16E_sI}\right) = -\frac{Fl}{2AE_s} + \frac{Fl^3}{24E_sI} \tag{16}$$

The Poisson's ratio is therefore given by:

$$\nu = \frac{\delta_{lateral}}{\delta_{uc}} = \frac{-\frac{Fl}{2AE_s} + \frac{Fl^3}{24E_sI}}{\frac{3Fl}{2AE_s} + \frac{Fl^3}{24E_sI}} = \frac{-12I + Al^2}{36I + Al^2} = \frac{-t^2 + l^2}{3t^2 + l^2} \tag{17}$$

In order to find the yield stress in the structure, first the maximum stress in each cell wall must be calculated. If the load F is applied to each unit cell, the normal compressive stress in edge CD is

$$\sigma_{max,CD} = -\frac{\frac{F}{2}}{\frac{A}{2}} = -\frac{F}{A} \tag{18}$$

and the normal stress in edge BC is:

$$\sigma_{BC} = \sigma_{BC,axial} \pm \sigma_{BC,bending} = -\frac{F}{2A}\frac{\sqrt{2}}{2} \pm \left[\frac{Mc}{I} - \frac{\left(\frac{F}{2}\frac{\sqrt{2}}{2}\right)lc}{I}\right] \tag{19}$$

where c is the distance between the neutral plane and the farthest portion of the beam cross-section. Substituting M from Eq. (5) gives:

$$\sigma_{BC,max} = -\frac{F}{2A}\frac{\sqrt{2}}{2} \pm \left[\frac{\frac{Fl\sqrt{2}}{8}c}{I} - \frac{\left(\frac{F}{2}\frac{\sqrt{2}}{2}\right)lc}{I}\right] = -\frac{F\sqrt{2}}{4A} - \frac{Fl\sqrt{2}c}{8I} \tag{20}$$

Considering Eq. (18) and Eq. (20), the maximum compressive stress in the structure is found by:

$$\sigma_{max} = max\left\{\frac{F}{A}, \quad \frac{F\sqrt{2}}{4A} + \frac{Fl\sqrt{2}c}{8I}\right\} \tag{21}$$

Our calculations showed that the second term is larger than the first term in all the relative densities. If an applied external stress $\frac{F}{(1+\sqrt{2})lb}$ on the unit cell creates the maximum local stress of $\frac{F\sqrt{2}}{4A} + \frac{Fl\sqrt{2}c}{8I}$ in the structure, the external stress σ_y which causes the maximum local stress in the structure reach σ_{y_s} can be found by a simple cross multiplication. By dividing the resulted relationship by σ_{y_s}, the relative yield stress of the structure can be found as

$$\sigma_{y_{rel}} = \frac{1}{(1+\sqrt{2})lb}\left[\frac{\sqrt{2}}{4A} + \frac{l\sqrt{2}c}{8I}\right]^{-1} = \frac{2\sqrt{2}\,t^2}{(1+\sqrt{2})(t+3l)l} \tag{22}$$

2.4. Timoshenko beam theory

The Timoshenko beam theory takes into account shear deformation and rotational inertia effects, making it suitable for describing the behaviour of thick beams. For a homogenous beam of constant cross-section, the Timoshenko beam governing equations are:

$$\frac{d^2}{dx^2}\left(E_s I \frac{d\varphi}{dx}\right) = q(x,t) \tag{23}$$

$$\frac{dw}{dx} = \varphi - \frac{1}{\kappa AG}\frac{d}{dx}\left(E_s I \frac{d\varphi}{dx}\right)$$

where φ is the angle of rotation of the normal to the mid-surface of the beam, w is the lateral displacement of the mid-surface, and κ is the shear coefficient factor. The shear coefficient factor is $10(1+\nu)/(12+11\nu)$ for a beam with rectangular cross-section (which is the case in this study). In a linear elastic Timoshenko beam, the bending moment M_{xx} and the shear force Q_x are related to the angle of rotation, φ, and the displacement, w, by

$$M_{xx} = -EI\frac{\partial \varphi}{\partial x} \tag{24}$$

$$Q_x = \kappa AG\left(-\varphi + \frac{\partial w}{\partial x}\right)$$

For a cantilever Timoshenko beam with a point load P at its free end, Eqs. (24) lead to

$$\delta = \frac{Pl^3}{3E_sI} + \frac{Pl}{\kappa AG_s} \qquad and \qquad \theta = \frac{Pl^2}{2E_sI} + \frac{P}{\kappa AG_s} \tag{25}$$

which have additional terms compared to those in the Euler-Bernoulli beam. However, for the beam with a concentrated moment M at its end, the displacement and rotation are identical to those of Euler-Bernoulli beam. As in the case of the Euler-Bernoulli beam theory, the rotations produced by the lateral load $P = F/2\cos\theta$ and moment M must be equal and opposite from which the value of M for a structure based on the Timoshenko beam theory can be determined:

$$\frac{Pl^2}{2E_sI} + \frac{P}{\kappa AG_s} = F\frac{\sqrt{2}}{4}\left[\frac{l^2}{2E_sI} + \frac{1}{\kappa AG_s}\right] = \frac{Ml}{E_sI} \qquad \Rightarrow \qquad M = F\frac{\sqrt{2}}{4}\left(\frac{l}{2} + \frac{E_sI}{\kappa AG_s l}\right) \tag{26}$$

The moment M tends to increase the length GC (Figure 3b) by

$$\delta_{BC_M} = \frac{F\frac{\sqrt{2}}{4}\left(\frac{l}{2} + \frac{E_sI}{\kappa AGl}\right)l^2}{2E_sI}\frac{\sqrt{2}}{2} = \frac{F}{8}\left(\frac{l^3}{2E_sI} + \frac{l}{\kappa AG_s}\right) \tag{27}$$

On the other hand, the lateral load $F/2\cos\theta$ tends to decrease the length GC (Figure 3b) by

$$\delta_{BC_{F,bending}} = F\frac{\sqrt{2}}{4}\left(\frac{l^3}{3E_sI} + \frac{l}{\kappa AG_s}\right)\frac{\sqrt{2}}{2} = \frac{F}{4}\left(\frac{l^3}{3E_sI} + \frac{l}{\kappa AG_s}\right) \tag{28}$$

The displacements resulted from the axial loads, i.e. $\delta_{BC_{F,axial}}$ and $\delta_{CC`}$ are identical to those for the Euler-Bernoulli beam theory. The total vertical displacement of the unit cell is therefore

$$\begin{aligned}\delta_{uc} &= 2\left(\delta_{CC`} + \delta_{BC_{F,axial}} + \delta_{BC_{F,bending}} - \delta_{BC_M}\right) \\ &= 2\left\{\frac{Fl}{2AE_s} + \frac{Fl}{4AE_s} + \frac{F}{4}\left(\frac{l^3}{3E_sI} + \frac{l}{\kappa AG_s}\right) - \frac{F}{8}\left(\frac{l^3}{2E_sI} + \frac{l}{\kappa A_{\ s}}\right)\right\} \\ &= \frac{3Fl}{2AE_s} + \frac{Fl}{4\kappa AG_s} + \frac{Fl^3}{24E_sI}\end{aligned} \tag{29}$$

Like before, the simple equation $E = \frac{F\,L_{uc}}{A_{uc}\delta_{uc}}$ can be used to find the elastic modulus of the octagonal honeycomb structure. Substituting Eq. (29), the elastic modulus of the octagonal honeycomb structure is

$$E = \frac{F}{b\left[\frac{3Fl}{2AE_s} + \frac{Fl}{4\kappa AG_s} + \frac{Fl^3}{24E_sI}\right]} \tag{30}$$

and the relative elastic modulus is

$$E_\mu = \frac{E}{E_s} = \frac{1}{b\left[\frac{3l}{2A} + \frac{l(1+\nu_s)}{2\kappa A} + \frac{l^3}{24I}\right]} = \frac{2\left(\frac{t}{l}\right)}{3 + \frac{1+\nu_s}{\kappa} + \left(\frac{l}{t}\right)^2} \tag{31}$$

To obtain the Poisson's ratio of the structure, it is first necessary to calculate its lateral displacement. The lateral displacement of the structure is twice the horizontal displacement of point C in Figure 3b, which is given by

$$\delta_{lateral} = 2\left(-\delta_{BC_{F,axial}} + \delta_{BC_{F,bending}} - \delta_{BC_M}\right) \tag{32}$$

Substituting Eqs. (10), (27), and (28) into Eq. (32) gives

$$\begin{aligned}\delta_{lateral} &= 2\left[\frac{-Fl}{4AE_s} + \frac{F}{4}\left(\frac{l^3}{3E_sI} + \frac{l}{\kappa AG}\right) - \frac{F}{8}\left(\frac{l^3}{2E_sI} + \frac{l}{\kappa AG}\right)\right] \\ &= \frac{-Fl}{2AE_s} + \frac{Fl(1+\nu_s)}{2\kappa AE_s} + \frac{Fl^3}{24E_sI}\end{aligned} \tag{33}$$

The Poisson's ratio is then easily found by:

$$\begin{aligned}\nu = \frac{\delta_{lateral}}{\delta} &= \frac{\frac{-Fl}{2AE_s} + \frac{Fl(1+\nu_s)}{2\kappa AE_s} + \frac{Fl^3}{24E_sI}}{\frac{3Fl}{2AE_s} + \frac{Fl}{4\kappa AG_s} + \frac{Fl^3}{24E_sI}} = \frac{-I\kappa + I(1+\nu_s) + \frac{A\kappa l^2}{12}}{3I\kappa + I(1+\nu_s) + \frac{A\kappa l^2}{12}} \\ &= \frac{-t^2 + l^2 + t^2\left(\frac{1+\nu_s}{\kappa}\right)}{3t^2 + l^2 + t^2\left(\frac{1+\nu_s}{\kappa}\right)}\end{aligned} \tag{34}$$

Now, we find the yield stress for the structure based on the Timoshenko beam theory. The normal stress in edge CD is

$$\sigma_{max,CD} = -\frac{F}{A} \tag{35}$$

and the normal stress in edge BC is:

$$\sigma_{BC} = \sigma_{BC,axial} \pm \sigma_{BC,bending} = -\frac{F}{2A}\frac{\sqrt{2}}{2} \pm \left[\frac{Mc}{I} - \frac{\left(\frac{F}{2}\frac{\sqrt{2}}{2}\right)lc}{I}\right] \tag{36}$$

$$= -\frac{F}{2A}\frac{\sqrt{2}}{2} \pm \left[\frac{F\frac{\sqrt{2}}{4}\left(\frac{l}{2} + \frac{2(1+\nu_s)I}{\kappa A l}\right)c}{I} - \frac{\left(\frac{F}{2}\frac{\sqrt{2}}{2}\right)lc}{I}\right]$$

The maximum compressive stress in the cell wall is therefore

$$\sigma_{BC,max} = \frac{F\sqrt{2}}{4A}\left[1 - \frac{2(1+\nu_s)c}{\kappa l}\right] + \frac{F\sqrt{2}lc}{8I} \tag{37}$$

Consequently, the maximum stress in the structure is found by:

$$\sigma_{max} = max\left\{\frac{F}{A}, \quad \frac{F\sqrt{2}}{4A}\left[1 - \frac{2(1+\nu_s)c}{\kappa l}\right] + \frac{F\sqrt{2}lc}{8I}\right\} \tag{38}$$

The calculations showed that the second term is larger than the first term in all the relative densities. A simple cross multiplication could be used to determine the relative yield stress in an octagonal unit cell based on the Timoshenko beam theory:

$$\sigma_{y_{rel}} = \frac{1}{(1+\sqrt{2})lb}\left[\frac{\sqrt{2}}{4A}\left[1 - \frac{2(1+\nu_s)c}{\kappa l}\right] + \frac{\sqrt{2}lc}{8I}\right]^{-1} \tag{39}$$

$$= \frac{1}{(1+\sqrt{2})}\frac{\frac{t}{l}}{\left[\frac{\sqrt{2}}{4}\left[1 - \frac{2(1+\nu_s)t}{2\kappa l}\right] + \frac{3\sqrt{2}l}{4t}\right]}$$

2.5. Buckling load

Since the honeycomb structures are usually used in compression, buckling instability can also cause sudden structural deformations which can lead to catastrophic failure of the honeycomb. The elastic buckling limit of the octagonal honeycomb can be obtained using the classical Euler's buckling theory. Since the Timoshenko and Euler-Bernoulli theories predict

similar deformations under axial loading, one buckling relationship will be obtained for both theories. The Euler's formula for buckling load of columns under compressive loading is:

$$P_{cr,column} = \frac{\pi^2 E_s I}{(KL)^2} \tag{40}$$

where KL is the effective length of the column and is $0.5L$ when both ends are fixed. In the octagonal honeycomb unit cell, the vertical edges are the most susceptible edges to buckling. These vertical edges can be considered as columns with both ends fixed, due to their purely transitional lateral movement in pre-buckling deformation. By substituting $KL = 0.5l$ in Eq. (40), the critical load of a unit cell under the compressive load F is given by

$$P_{cr,unit\ cell} = \frac{4\pi^2 E_s I}{l^2} \tag{41}$$

from which the critical stress is readily obtained

$$\sigma_{cr} = \frac{4\pi^2 E_s I}{l^2}\frac{1}{(1+\sqrt{2})lb} = \frac{4\pi^2}{(1+\sqrt{2})}\frac{E_s I}{bl^3} = \frac{\pi^2 E_s}{3(1+\sqrt{2})}\left(\frac{t}{l}\right)^3 \tag{42}$$

2.6. FE modelling

The main mechanism of deformation in the microstructure of a honeycomb structure is bending of the cell walls making the beam elements the natural choice for modelling them. They are computationally inexpensive and can be used to construct models with many cells [35]. The cell edges were discretized using the standard Timoshenko beam elements (element type 189 in ANSYS) that uses linear interpolation (two-node linear beam). Beams that were rigidly connected at the vertices mechanically represented all the edges in the honeycomb structure. In all the calculations, the cell edge material was assumed to be linear elastic with mechanical properties similar to the mechanical properties of the bulk PLA material determined in the experiments of cylindrical specimens.

The static nonlinear implicit solver available in ANSYS FE code was used for the calculations. Two types of models were created for the numerical modelling. The first model

was a small model consisting of three edges corresponding to 1/4 of a unit cell (Figure 4a). In this structure, all the degrees of freedom of the bottom edge were fixed and the right edge was only allowed to move transitionally. A concentred force F was applied at the top right side of the structure (Figure 4a).

The other model was a large lattice structure with several unit cells. The number of elements per cell wall was changed and no considerable difference was observed. However, the predicted results were affected by the number of unit cells in each direction of the FE model. The results of the lattice structure converged for lattice sizes larger than 9×9×9. A lattice structure size of 14×14×14 unit cells was chosenm. The lowermost part of the lattice structure was not allowed to move in the Y direction, while the uppermost part of the lattice structure was displaced downward in such a way that the structure underwent 0.2% strain (Figure 4b). The lowermost and the uppermost nodes were allowed to move in the X direction, to better capture the lateral behaviour of the structure (for example for obtaining the Poisson's ratio parameter). One of the lowermost nodes of the lattice structure was fixed in all the directions to prevent the rigid body motions of the structure. The effective elastic modulus was calculated using the simple equation $E = \frac{P_{lattice} L_{lattice}}{A_{Lattice} \delta_{lattice}} = \frac{P_{lattice}}{b\ \delta_{lattice}}$. To obtain the Poisson's ratio, the lateral displacement was divided by the axial displacement of the structure. For the yield stress, similar to the analytical solution, first the maximum stress in the structure was found and then inserted into a simple relationship for cross multiplication.

3. RESULTS

There were few variations in the load-displacement curves obtained for various samples with the same relative density (Figure 6). The stress levels and failure loads were several times higher for specimens with higher values of relative density as compared to those with the lowest values of relative density (Figure 6). All of the octagonal test samples showed 45º

failure patterns (Figure 7). Comparison of the analytical solutions and the computational results showed that the FE models and both the analytical models give close results in terms elastic modulus Poisson's ratio, and yield stress, especially for relative densities smaller than 20% (Figure 8a-c). The presence of porosity in the honeycomb structure decreases the relative elastic modulus and relative yield stress severely, in such a way that even at relative densities as large as 50%, the relative elastic modulus and relative yield stress did not exceed 15% of those in the bulk material (Figure 8a,c).

At relative densities larger than 25%, the numerical and analytical values of elastic modulus started to deviate from each other (Figure 8a). However, even at large relative densities, each set of analytical (Euler-Bernoulli and Timoshenko) and numerical (lattice structure and single unit cell) elastic moduli showed very close predictions. The experimental values of the elastic modulus were very close to the numerical predictions for three out of four relative densities (Figure 8a). There was a better agreement between computational results and the analytical solutions based on the Timoshenko beam theory (Figure 8a).

Both analytical models and the computational models predicted Poisson's ratios that started from 1 for very low values of relative density and gradually decreased (Figure 8b). Similar to case of elastic modulus, the analytical values of Poisson's ratio based on the Timoshenko beam theory were closer to the numerical results for all values of relative density (as compared to those based on the Euler-Bernoulli beam theory). At a relative density of 60%, the Poisson's ratio of the octagonal structure decreased to ≈0.4 (Figure 8b).

Similar to the case of elastic modulus and Poisson's ratio, the predicted values of yield stress are very close for both FE models (Figure 8c). The experimental values of the yield stress are always lower than the yield stress values predicted by both analytical solutions and computational models (Figure 8c). Reviewing Figure 8a-c shows that the elastic modulus,

Poisson's ratio, and yield stresses predicted by the Timoshenko analytical solution is lower, higher, and higher, respectively, than those calculated by the Euler-Bernoulli analytical solution.

4. DISCUSSION

In this study, two types of FE models were used. A simple model similar to the one considered for obtaining the analytical relationships and a large 2D tessellated structure with a high number of cell walls (1204 cell walls). The elastic moduli obtained from both computational models were very close with a maximum difference below 4% even for a relative density as large as 60%.

It is customary to present the analytical relationships used for prediction of mechanical properties in terms of the relative density, μ, rather than t/l ratio. Since the exact relative density formula (Eq. (4)) obtained here is a quadratic polynomial, it cannot be readily inserted into the relationships obtained for the elastic modulus, yield stress, and Poisson's ratio. However, the approximate relative density formula (i.e. Eq. (1)) may be inserted into the elastic property equations to derive those equations as a function of (approximate) relative density, μ. The problem is that in the approximate formula for relative density, the material located in the vertices of the cells are counted multiple times, which can lead to inaccurate results [36] . Therefore, before doing that, it is necessary to find the influence of multiple counting of material located in the cell vertices on the obtained relative density. In one of our previous studies [36], the effect of multiple counting on the elastic properties of 3D open-cell porous structures with different unit cell types was investigated. As it can be seen in Figure 10, as the ratio of t/l increases, the difference between the calculated relative densities increases. However, the relative densities do not deviate from each other more than 20% even for a large t/l ratio such as 0.5.

The main reason for the 45º failure band can be the fact that inclined walls are the critical edges in the octagonal structure. The computational results as well as the analytical results (Equation (38) and (39)) both show the fact that the inclined edges are the parts with the most vulnerability.

All the experimental data points for both the elastic modulus and yield stress correlate well with the numerical and analytical values (Figure 8). The only exception is the experimental results corresponding to the weakest sample (i.e. the sample with $t/l = 0.2727$). Compared to the numerical and analytical results, the experimentally determined values of elastic properties are very small for the samples with this relative density. The additively manufactured porous structures usually have relatively rough external surfaces. The roughness of the samples with different relative densities is not essentially different because the roughness of the product is mostly determined by the manufacturing parameters of the manufacturing device rather than the geometry of the product. Therefore, the larger the thickness of the cell walls, the lower the effect of surface roughness. This is because the proportion of completely filled central parts to the weaker external parts in the cross-section of the cell walls increases by increasing the thickness of the cell walls. This fact is verified by our experimental results: the experimental/analytical correlation is much improved for higher relative densities. The reason behind the very small mechanical properties of the most porous structure (i.e. the sample with $t/l = 0.2727$) might be the fact that in this structure, the cell walls are much thinner than the weaker external parts of the cell as compared to the thickness of the completely filled central parts. Therefore, a large fraction of the cross-section of the cell walls is composed of external weak parts that cannot bear load.

Deformations of open-cell porous materials are usually dominated by mechanisms such as linear elastic deformation, buckling of the edges, plasticity of the edges, interaction of neighbour cell edges, etc. In the elastic regime, the two mechanisms of local yielding of the

edges and buckling of the edges parallel to the loading direction are the mechanisms dominating the start of plateau region in the stress-strain curve of the porous structure. It is necessary to determine which of the two failure mechanisms occur first. Plotting the yield stress (Eq. (39)) against the buckling stress (Eq. (42)) demonstrated that the buckling stress of this structure (if it is made of steel) is much smaller than its yield stress (Figure 9).

After the advent of additive manufacturing techniques, they have been mostly used in production of 3D complex geometries that could not be otherwise manufactured. Among the different 3D foams, structures such as diamond [37], rhombic dodecahedron [36], truncated cuboctahedron [38, 39], truncated cube [40], octahedral [41], and rhombicuboctahedron [42] have been previously studied by our group as candidates for biomedical implants used in orthopedics. Conventional manufacturing techniques for the production of honeycombs have several limitations. First, honeycombs with very small cell sizes cannot be produced. Second, since honeycomb cell walls are usually shaped using metal forming methods, their thickness to cell size ratio cannot be larger than a specific value. Third, for each unit cell type, a different production method is necessary and production of honeycombs with arbitrary geometry is not always possible. Additive manufacturing (AM) techniques overcome all the noted limitations to a great extent. In recent years, selective laser melting (SLM) has been used to create hexagonal honeycombs [43, 44]. The octagonal honeycomb studied in this paper is one of the many types of honeycombs that can be produced using additive manufacturing.

In this study, the elastic modulus, yield strength, and buckling stress of the in-plane deformation of the octagonal honeycomb were expressed in terms of relative density to enable direct comparison of the obtained results with other types of honeycombs. In a study carried out by Wang and McDowell [28], several geometries such as square, triangular,

hexagonal, Kagome, diamond, and mixed were considered for honeycomb structures and were investigated analytically using Euler-Bernoulli beam theory. Comparison of the elastic properties of the octagonal honeycomb with other types of honeycombs provides good insight on the potential use of this honeycomb to the designer. Considering Figure 11, it is obvious that the octagonal honeycomb has a relatively smaller yield stress and elastic modulus compared to most of the above-mentioned geometries. In fact, the response of an octagonal honeycomb is very close to that of a hexagonal honeycomb which is the most prevalent geometry for honeycombs. Although the elastic modulus and yield stress of an octagonal honeycomb is very similar to hexagonal honeycomb, the symmetry of the microstructure of octagonal honeycomb in its two main directions can lead to more similar post-yielding deformation in its two main directions than is the case for the post yielding deformation of the two main directions of hexagonal honeycomb. Figure 12 shows the different post-yielding deformation modes of a hexagonal honeycomb in its two main in-plane directions. The square honeycombs have the highest elastic properties among all the geometries. It must be stated that the low elastic properties of the octagonal honeycomb is not necessarily a weakness for this type of structures. In fact, depending on the application of this structure, such as energy absorption in in-plane or out-of-plane loading, the low elastic properties of the honeycomb can be insignificant or even desirable. In most cellular structures, the energy absorption capacity ability of the structure is the main criteria for selection of a specific design. Therefore, investigation of the response of octagonal honeycombs in the post-elastic region is necessary for implementing this geometry in practice.

In the earliest phases of tissue regeneration, when blood vessels are not yet regenerated, nutrition and oxygenation of the cells must occur through diffusion. If honeycomb structures are used for tissue regeneration applications, the entire plane of their two-dimensional structure should be in contact with the culture media from both sides to ensure diffusion can

effectively perform the required mass transport. Even then, the thickness of the honeycombs cannot exceed what can be effectively nurtured and oxygenated through diffusion. Additive manufacturing techniques similar to the ones used in the current study could be employed to introduce holes in the walls of the honeycomb structure with very large thicknesses. However, the analytical formulas derived here should be then modified to take the presence of those holes into account.

5. CONCLUSIONS

In this study, analytical relationships were obtained for the mechanical properties (i.e. elastic modulus, Poisson's ratio, yield stress, and buckling stress) of octagonal honeycomb structures. Both the Euler-Bernoulli and Timoshenko beam theories were considered for deriving the analytical relationships. Two FE models were also created, one consisting of only ¼ of a unit cell and the other consisting of a large set of unit cells. The simulation results obtained from the two FE models revealed that their results were very close and the difference between the results was less than 4% for elastic modulus. Comparison of the Euler-Bernoulli and Timoshenko analytical results in one hand and the numerical results in the other hand showed that the FE models and the analytical Timoshenko results were close to each other in terms of all the properties of elastic modulus, Poisson's ratio and yield stress, especially at relative densities smaller than 25%. Plotting the yield stress against the buckling stress demonstrated that the buckling stress of this structure made of steel is much smaller than its yield stress. The results of the Timoshenko analytical solution as well as the two finite element models also showed good correlation with the experimental results. Finally, the elastic properties of the octagonal honeycomb structure was compared to those of honeycomb structures having square, triangular, hexagonal, mixed, diamond, and Kagome unit cell shapes. The octagonal honeycomb showed yield stress and elastic modulus values close to those of hexagonal honeycomb and lower than the other above-mentioned honeycombs.

REFERENCES

1. Tanaka, M., K. Yoshizawa, A. Tsuruma, H. Sunami, S. Yamamoto, and M. Shimomura, *Formation of hydroxyapatite on a self-organized 3D honeycomb-patterned biodegradable polymer film.* Colloids and Surfaces A: Physicochemical and Engineering Aspects, 2008. **313**: p. 515-519.
2. Yang, N., L. Gao, and K. Zhou, *Simple method to generate and fabricate stochastic porous scaffolds.* Materials Science and Engineering: C, 2015. **56**: p. 444-450.
3. Gibson, L.J. and M.F. Ashby, *Cellular solids: structure and properties*. 1997: Cambridge university press.
4. Chantarapanich, N., P. Puttawibul, S. Sucharitpwatskul, P. Jeamwatthanachai, S. Inglam, and K. Sitthiseripratip, *Scaffold library for tissue engineering: a geometric evaluation.* Computational and mathematical methods in medicine, 2012. **2012**.
5. SU, X.-b., Y.-q. YANG, Y. Peng, and J.-f. SUN, *Development of porous medical implant scaffolds via laser additive manufacturing.* Transactions of Nonferrous Metals Society of China, 2012. **22**: p. s181-s187.
6. Van Bael, S., Y.C. Chai, S. Truscello, M. Moesen, G. Kerckhofs, H. Van Oosterwyck, J.-P. Kruth, and J. Schrooten, *The effect of pore geometry on the in vitro biological behavior of human periosteum-derived cells seeded on selective laser-melted Ti6Al4V bone scaffolds.* Acta biomaterialia, 2012. **8**(7): p. 2824-2834.
7. Singh, I., *The architecture of cancellous bone.* Journal of anatomy, 1978. **127**(Pt 2): p. 305.
8. Li, X., C. Wang, W. Zhang, and Y. Li, *Fabrication and compressive properties of Ti6Al4V implant with honeycomb-like structure for biomedical applications.* Rapid Prototyping Journal, 2010. **16**(1): p. 44-49.
9. Bae, J.-H., H.-R. Song, H.-J. Kim, H.-C. Lim, J.-H. Park, Y. Liu, and S.-H. Teoh, *Discontinuous release of bone morphogenetic protein-2 loaded within interconnected pores of honeycomb-like polycaprolactone scaffold promotes bone healing in a large bone defect of rabbit ulna.* Tissue Engineering Part A, 2011. **17**(19-20): p. 2389-2397.
10. Kakudo, N., A. Shimotsuma, S. Miyake, S. Kushida, and K. Kusumoto, *Bone tissue engineering using human adipose-derived stem cells and honeycomb collagen scaffold.* Journal of Biomedical Materials Research Part A, 2008. **84**(1): p. 191-197.
11. Rodriguez, A.P., L. Missana, H. Nagatsuka, M. Gunduz, H. Tsujigiwa, R. Rivera, and N. Nagai, *Efficacy of atelocollagen honeycomb scaffold in bone formation using KUSA/A1 cells.* Journal of Biomedical Materials Research Part A, 2006. **77**(4): p. 707-717.
12. George, J., Y. Kuboki, and T. Miyata, *Differentiation of mesenchymal stem cells into osteoblasts on honeycomb collagen scaffolds.* Biotechnology and bioengineering, 2006. **95**(3): p. 404-411.
13. Gibson, L., M. Ashby, G. Schajer, and C. Robertson, *The mechanics of two-dimensional cellular materials.* Proceedings of the Royal Society of London. A. Mathematical and Physical Sciences, 1982. **382**(1782): p. 25-42.
14. Papka, S.D. and S. Kyriakides, *In-plane compressive response and crushing of honeycomb.* Journal of the Mechanics and Physics of Solids, 1994. **42**(10): p. 1499-1532.
15. Papka, S.D. and S. Kyriakides, *In-plane crushing of a polycarbonate honeycomb.* International Journal of Solids and Structures, 1998. **35**(3): p. 239-267.
16. Karakoç, A., K. Santaoja, and J. Freund, *Simulation experiments on the effective in-plane compliance of the honeycomb materials.* Composite Structures, 2013. **96**: p. 312-320.

17. Foo, C.C., G.B. Chai, and L.K. Seah, *Mechanical properties of Nomex material and Nomex honeycomb structure.* Composite structures, 2007. **80**(4): p. 588-594.
18. Scarpa, F., P. Panayiotou, and G. Tomlinson, *Numerical and experimental uniaxial loading on in-plane auxetic honeycombs.* The Journal of Strain Analysis for Engineering Design, 2000. **35**(5): p. 383-388.
19. Papka, S.D. and S. Kyriakides, *Experiments and full-scale numerical simulations of in-plane crushing of a honeycomb.* Acta Materialia, 1998. **46**(8): p. 2765-2776.
20. Zhu, H.X. and N. Mills, *The in-plane non-linear compression of regular honeycombs.* International Journal of Solids and Structures, 2000. **37**(13): p. 1931-1949.
21. Hedayati, R., M. Sadighi, M. Mohammadi Aghdam, and A.A. Zadpoor, *Mechanical Properties of Additively Manufactured Thick Honeycombs.* Materials, 2016. **9**(8): p. 613.
22. Ruan, D., G. Lu, B. Wang, and T. Yu, *In-plane dynamic crushing of honeycombs—a finite element study.* International Journal of Impact Engineering, 2003. **28**(2): p. 161-182.
23. Chung, J. and A.M. Waas, *Compressive response of honeycombs under in-plane uniaxial static and dynamic loading, Part 2: simulations.* AIAA journal, 2002. **40**(5): p. 974-980.
24. Sun, Y. and N.M. Pugno, *In plane stiffness of multifunctional hierarchical honeycombs with negative Poisson's ratio sub-structures.* Composite Structures, 2013. **106**: p. 681-689.
25. Grediac, M., *A finite element study of the transverse shear in honeycomb cores.* International journal of solids and structures, 1993. **30**(13): p. 1777-1788.
26. Guo, X.E. and L.J. Gibson, *Behavior of intact and damaged honeycombs: a finite element study.* International Journal of Mechanical Sciences, 1999. **41**(1): p. 85-105.
27. Zheng, Z., J. Yu, and J. Li, *Dynamic crushing of 2D cellular structures: a finite element study.* International Journal of Impact Engineering, 2005. **32**(1): p. 650-664.
28. Wang, A.-J. and D. McDowell, *In-plane stiffness and yield strength of periodic metal honeycombs.* Journal of Engineering Materials and Technology, 2004. **126**(2): p. 137-156.
29. Torquato, S., L. Gibiansky, M. Silva, and L. Gibson, *Effective mechanical and transport properties of cellular solids.* International Journal of Mechanical Sciences, 1998. **40**(1): p. 71-82.
30. Gulati, S., *Effects of cell geometry on thermal shock resistance of catalytic monoliths*. 1975, SAE Technical Paper.
31. El-Sayed, F.A., R. Jones, and I. Burgess, *A theoretical approach to the deformation of honeycomb based composite materials.* Composites, 1979. **10**(4): p. 209-214.
32. Masters, I. and K. Evans, *Models for the elastic deformation of honeycombs.* Composite structures, 1996. **35**(4): p. 403-422.
33. Goswami, S., *On the prediction of effective material properties of cellular hexagonal honeycomb core.* Journal of reinforced plastics and composites, 2006. **25**(4): p. 393-405.
34. Balawi, S. and J. Abot, *A refined model for the effective in-plane elastic moduli of hexagonal honeycombs.* Composite Structures, 2008. **84**(2): p. 147-158.
35. Daxner, T., *Finite element modeling of cellular materials*, in *Cellular and Porous Materials in Structures and Processes*. 2010, Springer. p. 47-106.
36. Hedayati, R., M. Sadighi, M. Mohammadi-Aghdam, and A.A. Zadpoor, *Effect of mass multiple counting on the elastic properties of open-cell regular porous biomaterials.* Materials & Design, 2016. **89**: p. 9–20.

37. Ahmadi, S., G. Campoli, S. Amin Yavari, B. Sajadi, R. Wauthlé, J. Schrooten, H. Weinans, and A.A. Zadpoor, *Mechanical behavior of regular open-cell porous biomaterials made of diamond lattice unit cells.* Journal of the mechanical behavior of biomedical materials, 2014. **34**: p. 106-115.
38. Hedayati, R., M. Sadighi, M. Mohammadi-Aghdam, and A. Zadpoor, *Mechanical behavior of additively manufactured porous biomaterials made from truncated cuboctahedron unit cells.* International Journal of Mechanical Sciences, 2016. **106**: p. 19-38.
39. Ahmadi, S., S. Yavari, R. Wauthle, B. Pouran, J. Schrooten, H. Weinans, and A. Zadpoor, *Additively manufactured open-cell porous biomaterials made from six different space-filling unit cells: the mechanical and morphological properties.* Materials, 2015. **8**(4): p. 1871-1896.
40. Hedayati, R., M. Sadighi, M. Mohammadi-Aghdam, and A.A. Zadpoor, *Mechanical properties of regular porous biomaterials made from truncated cube repeating unit cells: analytical solutions and computational models.* Materials Science and Engineering: C, 2016. **60**: p. 163-183.
41. Hedayati, R., M. Sadighi, and A. Zadpoor, *Analytical relationships for the mechanical properties of additively manufactured porous biomaterials based on octahedral unit cells.* Submitted, 2015.
42. Hedayati, R., M. Sadighi, M. Mohammadi-Aghdam, and A.A. Zadpoor, *Mechanics of additively manufactured porous biomaterials based on the rhombicuboctahedron unit cell.* Journal of the Mechanical Behavior of Biomedical Materials, 2016. **53**: p. 272–294.
43. Chantarapanich, N., A. Laohaprapanon, S. Wisutmethangoon, P. Jiamwatthanachai, P. Chalermkarnnon, S. Sucharitpwatskul, P. Puttawibul, and K. Sitthiseripratip, *Fabrication of three-dimensional honeycomb structure for aeronautical applications using selective laser melting: a preliminary investigation.* Rapid Prototyping Journal, 2014. **20**(6): p. 551-558.
44. Rehme, O. and C. Emmelmann, *Selective Laser Melting of Honeycombs with Negative Poisson's Ratio.* Journal of Laser Micro/Nanoengineering, 2009. **4**: p. 128-134.

Figure captions

Figure 1- Dimensions of an octagonal unit cell
Figure 2- A 2D cut showing an octagonal unit cell before and after deformation under compressive loading
Figure 3- The free body diagram and deformation of (a) 1/4 portion of a unit cell, and (b) the inclined edge under compressive loading
Figure 4- The geometries, applied loads, and applied boundary conditions used in the (a) single unit cell, and (b) lattice FE octagonal structure
Figure 5- Octagonal honeycomb samples with (a) t/l=0.2727, (b) t/l=0.4091, (c) t/l=0.5454, and (d) t/l=0.6817
Figure 6- Load-displacement curves of octagonal honeycombs with different t/l ratios
Figure 7- 45º failure bands formed in honeycomb samples with (a) t/l=0.2727 and (b) t/l=0.5454
Figure 8- Variation of (a) relative elastic modulus, (b) Poisson's ratio, and (c) relative yield stress vs. relative density for octagonal honeycomb
Figure 9- Variation of yield and buckling stresses vs. relative density for octagonal honeycomb
Figure 10- Comparison of exact and approximate formulas for relative density versus the t/l ratio
Figure 11- Comparison of (a) elastic modulus, and (b) yield stress of the octagonal honeycomb with other types of honeycombs
Figure 12- Different post-yielding deformation modes of the two main directions of a hexagonal honeycomb: (a) an undeformed aluminium honeycomb, (b) the post-yielding deformation of the honeycomb in the $X1$ direction, and (c) the post-yielding deformation of the honeycomb in the $X2$ direction [2].

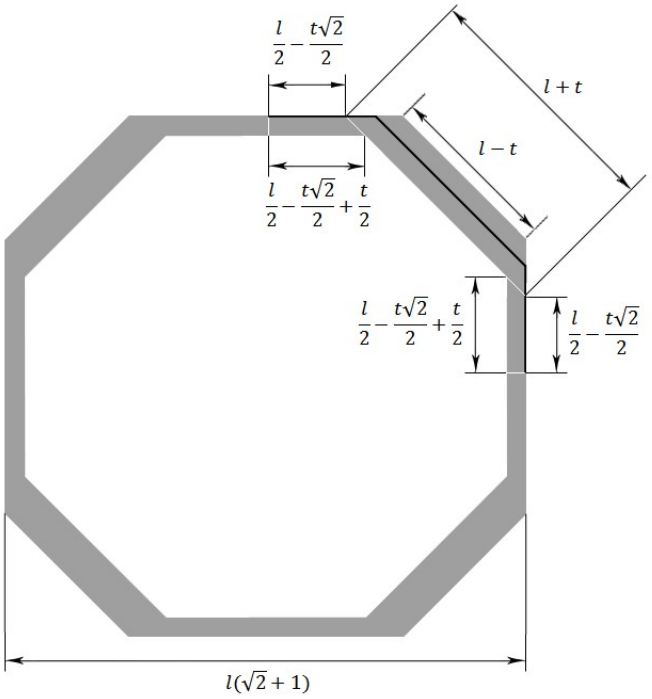

Figure 1- Dimensions of an octagonal unit cell

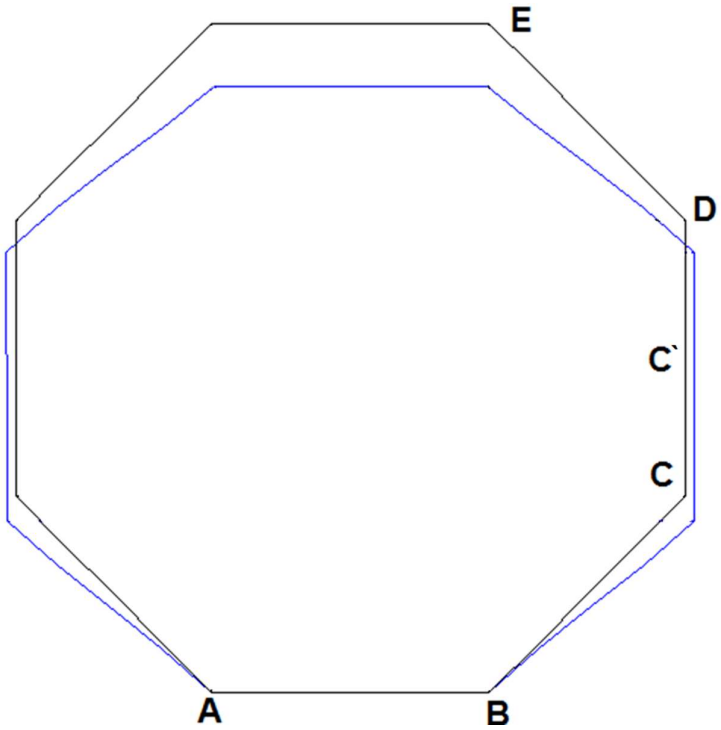

Figure 2- A 2D cut showing an octagonal unit cell before and after deformation under compressive loading

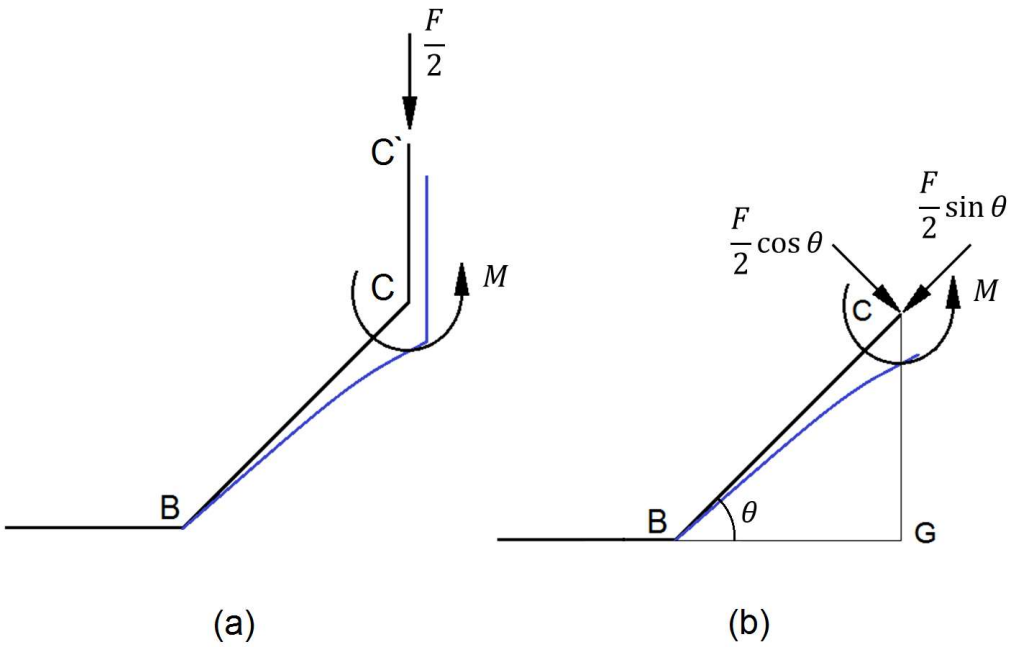

Figure 3- The free body diagram and deformation of (a) 1/4 portion of a unit cell, and (b) the inclined edge under compressive loading

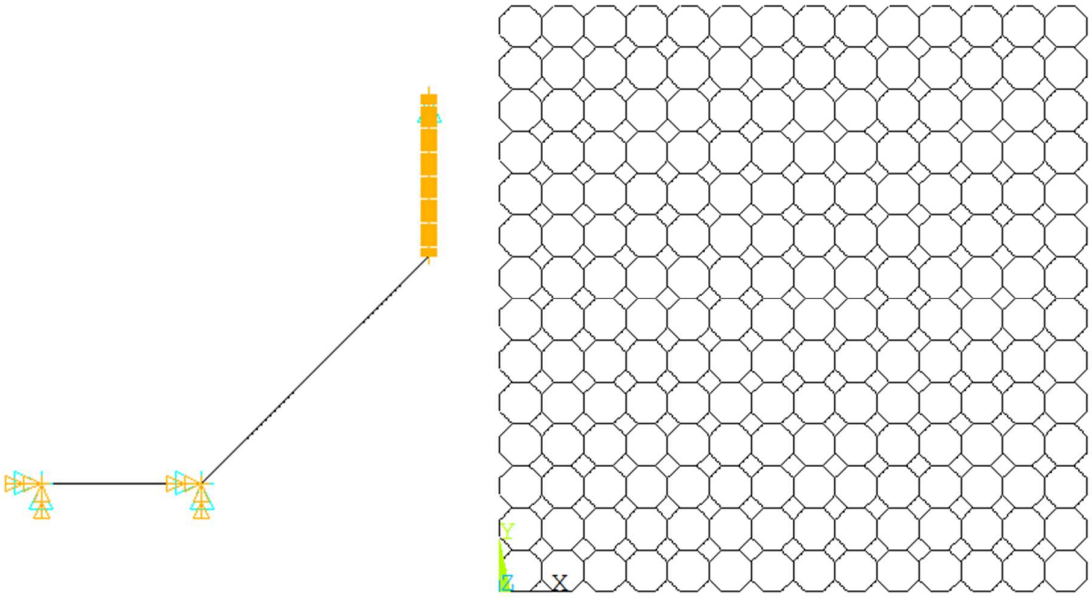

(a) (b)

Figure 4- The geometries, applied loads, and applied boundary conditions used in the (a) single unit cell, and (b) lattice FE octagonal structure

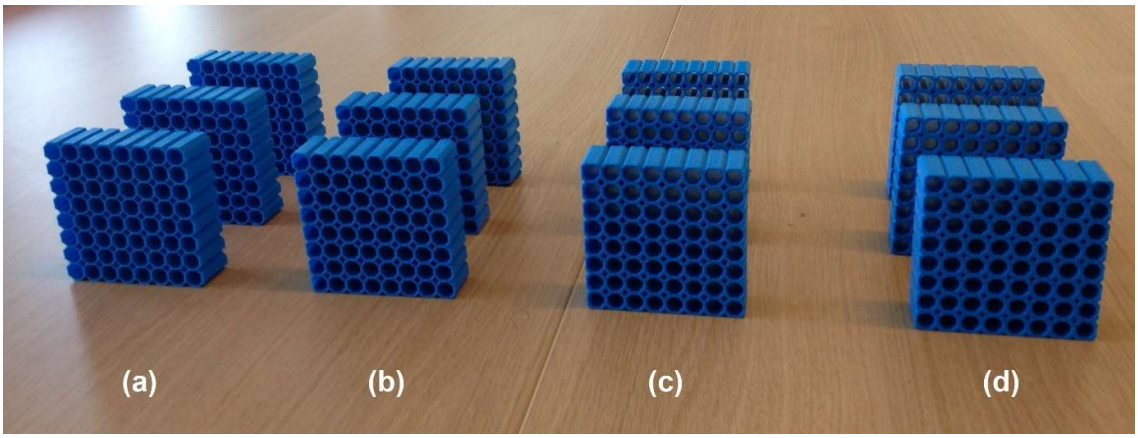

Figure 5- Octagonal honeycomb samples with (a) t/l=0.2727, (b) t/l=0.4091, (c) t/l=0.5454, and (d) t/l=0.6817

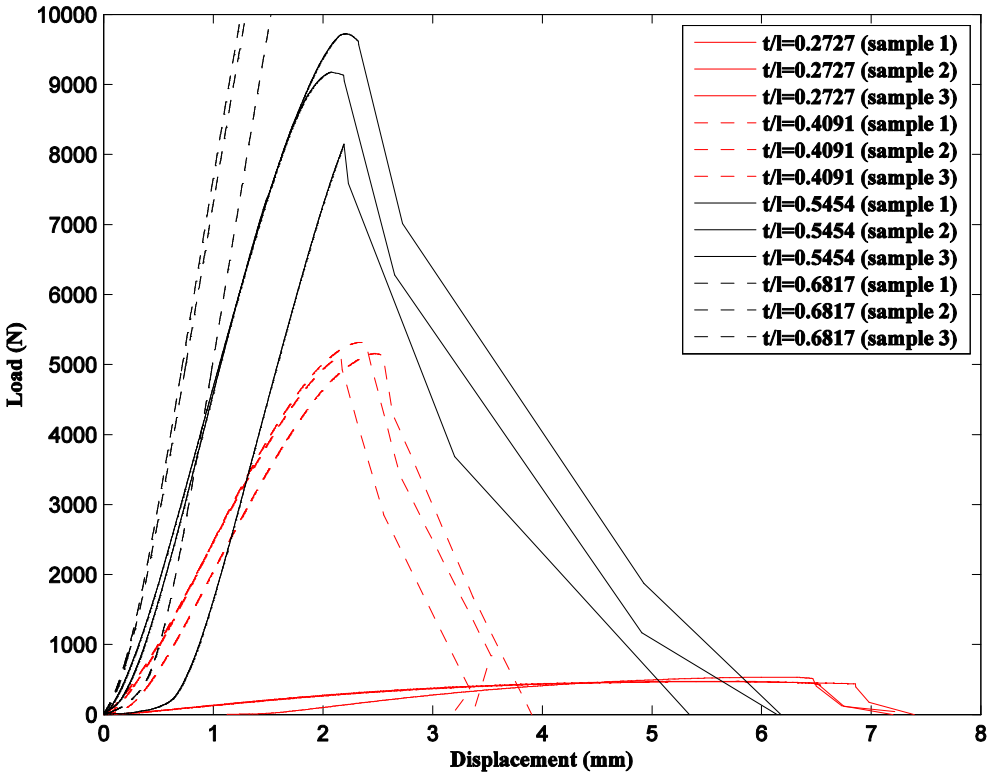

Figure 6- Load-displacement curves of octagonal honeycombs with different t/l ratios

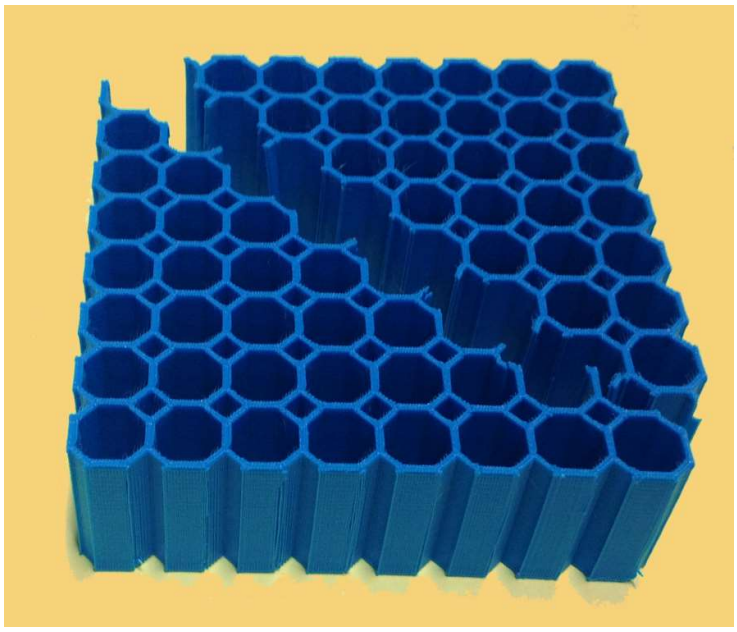

(a)

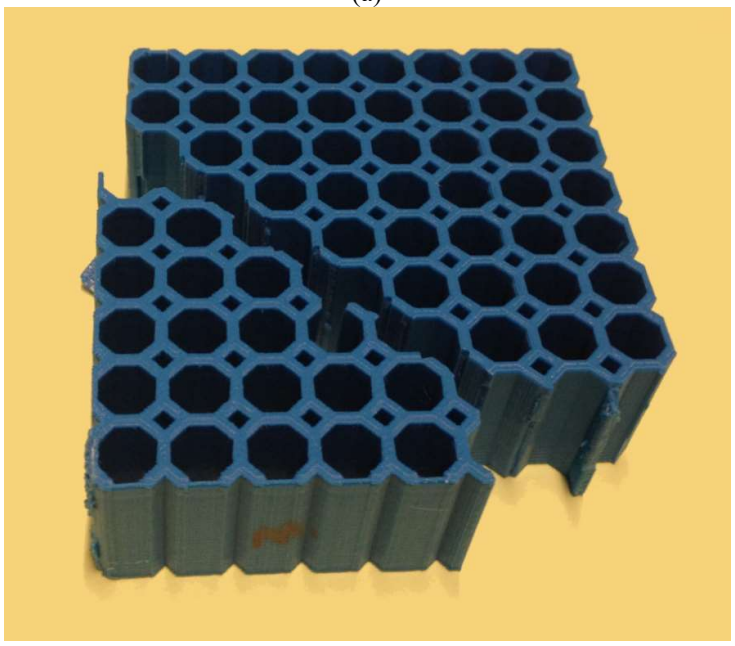

(b)

Figure 7- 45° failure bands formed in honeycomb samples with (a) t/l=0.2727 and (b) t/l=0.5454

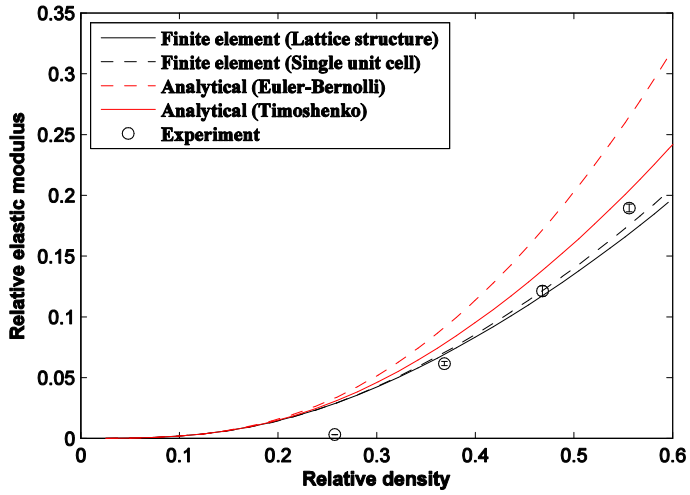

(a)

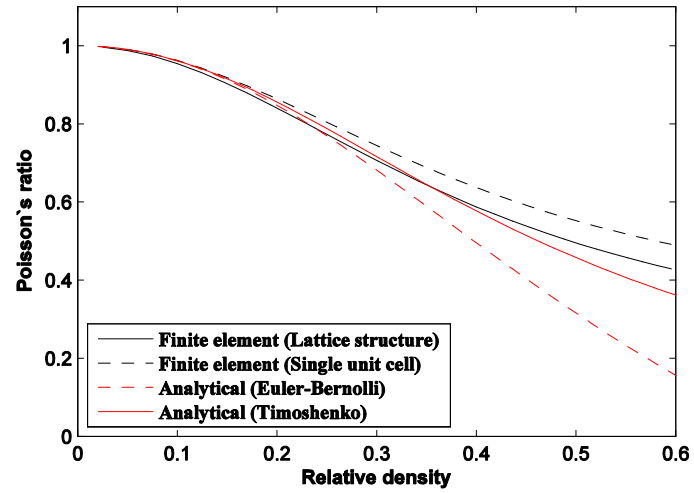

(b)

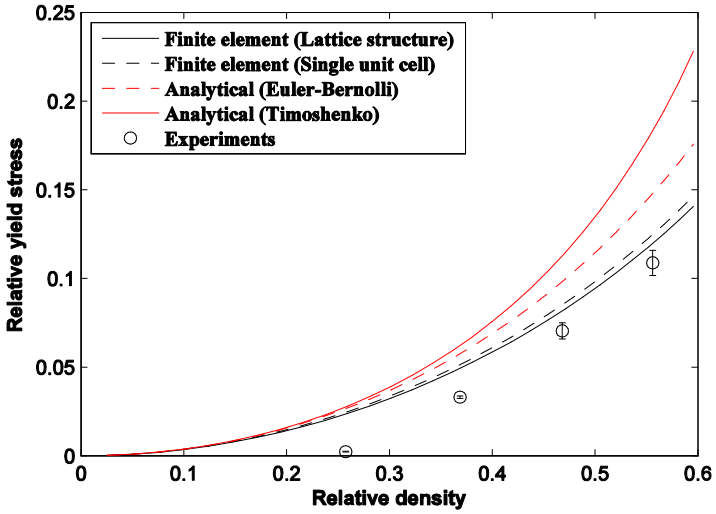

(c)

Figure 8- Variation of (a) relative elastic modulus, (b) Poisson's ratio, and (c) relative yield stress vs. relative density for octagonal honeycomb

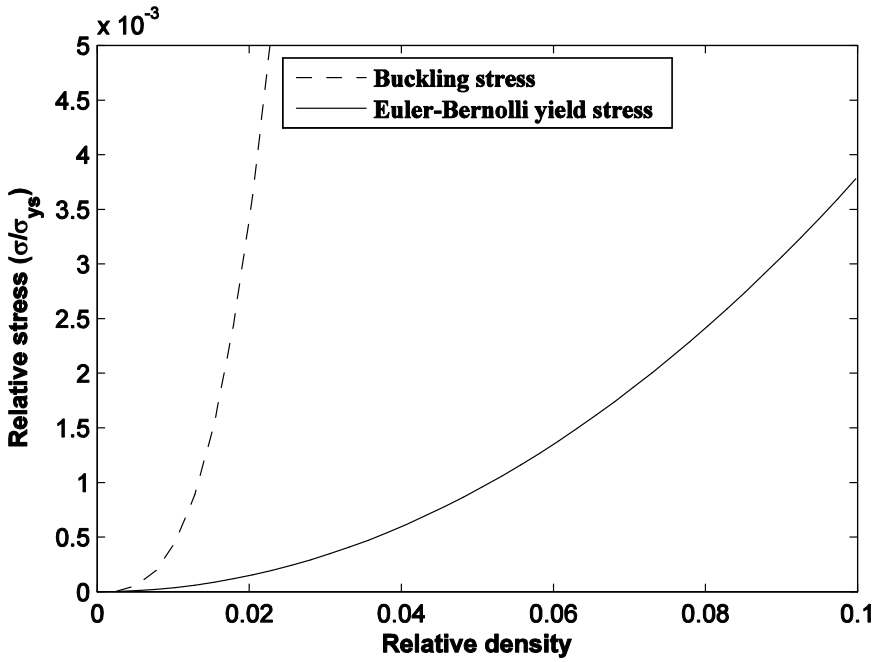

Figure 9- Variation of yield and buckling stresses vs. relative density for octagonal honeycomb

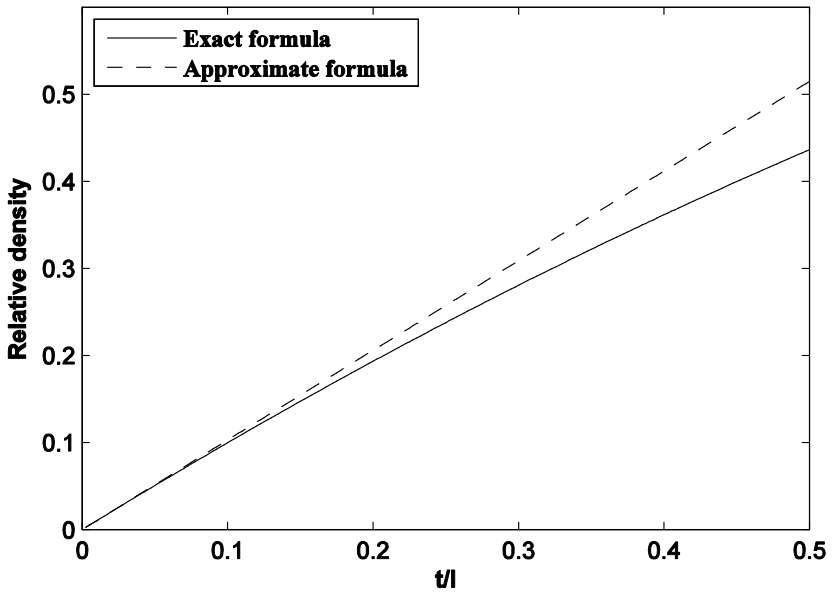

Figure 10- Comparison of exact and approximate formulas for relative density versus the t/l ratio

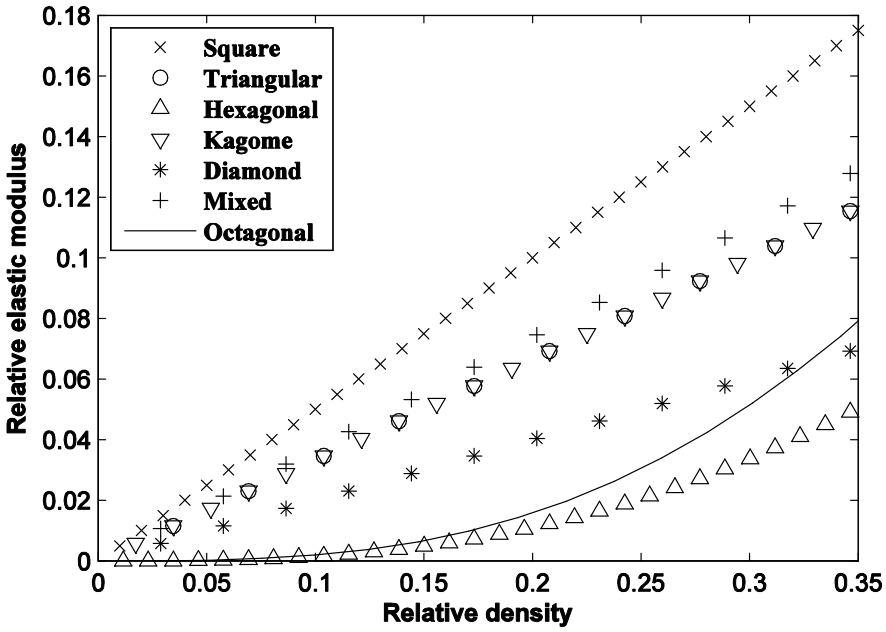

(a)

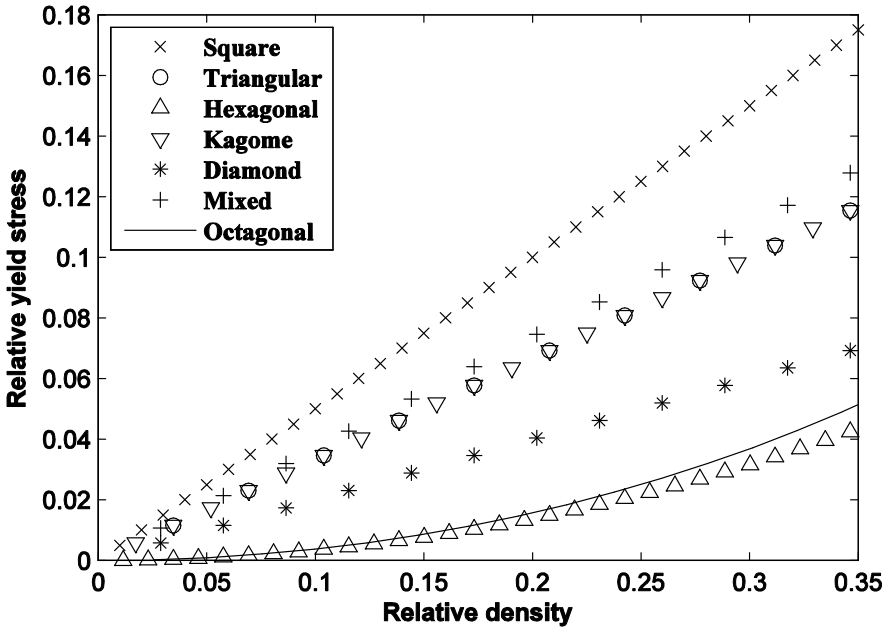

(b)

Figure 11- Comparison of (a) elastic modulus, and (b) yield stress of the octagonal honeycomb with other types of honeycombs

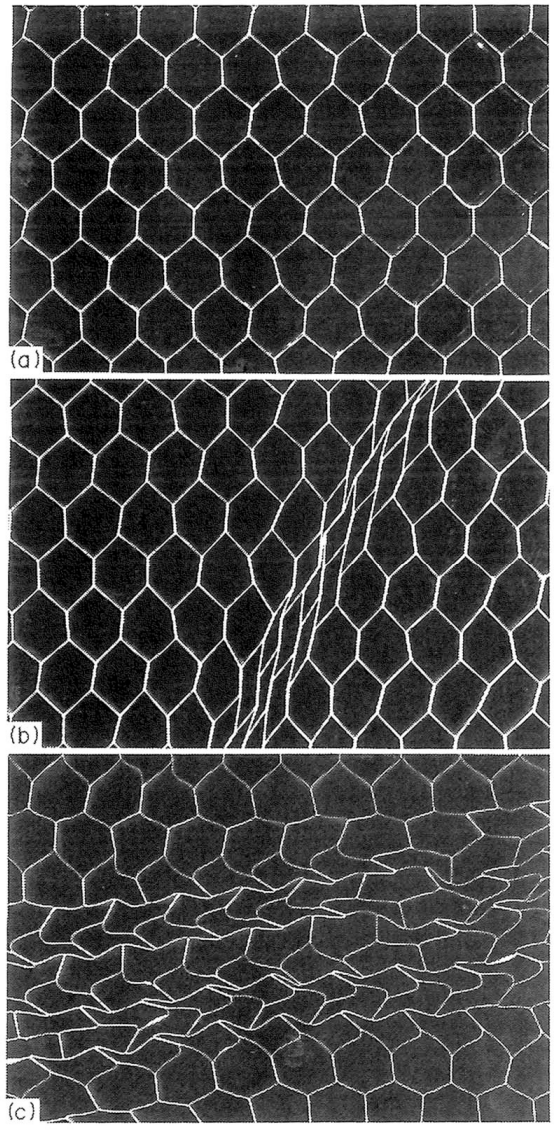

Figure 12- Different post-yielding deformation modes of the two main directions of a hexagonal honeycomb: (a) an undeformed aluminium honeycomb, (b) the post-yielding deformation of the honeycomb in the X_1 direction, and (c) the post-yielding deformation of the honeycomb in the X_2 direction [3].